J Mater Sci (2006) 41:7628–7635
DOI 10.1007/s10853-006-0855-4

Influence of solvents on the synthesis and electrochemical properties of $Li[Li_{1/5}Ni_{1/10}Co_{1/5}Mn_{1/2}]O_2$ for the applications in lithium-ion batteries

K. S. Park · C. H. Song · A. Manuel Stephan · S. K. Jeong · K. S. Nahm · S. M. Oh · Y. G. Kim

Received: 13 September 2005 / Accepted: 23 December 2005 / Published online: 11 October 2006

Abstract The solid solution of $Li[Li_{1/5}Ni_{1/10}Co_{1/5}Mn_{1/2}]O_2$ was synthesized using starting materials with two different functional groups (hydroxide and acetate) in the presence of a reaction medium ethanol or acetone using solid-state reaction method. The prepared samples were found to posses layered structure and their electrochemical properties were greatly influenced by the functional group of the starting materials. The samples which were prepared with same functional group offered better electrochemical properties and addition of solvents during the ball milling of the samples has considerably enhanced the diffusivity of the chemical species in the layered compound. The electrochemical properties and the influence of starting materials on the added solvents are discussed.

Introduction

In the recent past, many reports appear on the synthesis of solid solutions with layered manganese oxides, whose structure is very stable [1–7]. The solid solution oxides were synthesized with varying substituted transition metals and their composition. In general, the solid solution oxides were synthesized with typical rhombohedral structure (S.G.: R $\bar{3}$ m), and delivered high discharge capacity with stable cycle life [4–7]. Especially, an increase of the initial discharge capacity has been observed from the solid solutions with Li ion in their transition metal layers [1–4].

Most of the solid solutions have been mainly synthesized using a sol–gel method [1–7]. A very few literatures report the preparation of the materials using solid-state reaction method [8, 9]. The solid-state reaction is a commercially employed method for the production of large-scale lithiated mixed oxides. But this process has some disadvantages, such as poor stoichiometry and particles of larger size due to the inhomogeneous mixing of solid-phase reactants. In the solid-state reaction method, the enhancement of the solid-phase diffusion rate is an important factor to obtain materials with improved electrochemical properties. This can be achieved mainly by calcinating samples in a pressurized pellet form [8] or by synthesizing at higher temperatures [9]. However, the high temperature synthesis frequently causes the sublimation of Li ion from lithium metal oxides, whereas the pressurized sample synthesis needs longer synthesis time. There are a very few reports, which describe the use of alcohol or alcohol derivatives to improve the solid-phase diffusion in the solid-state reaction. Sakurai et al. [10] reported that they could synthesize α-$LiFeO_2$ phase at low temperatures less than 250 °C via H^+/Li^+ ionic exchange reaction by using alcohols and their derivatives as a reaction medium. So far to the best of our knowledge only a very few reports are available on the synthesis of layered manganese oxides using alcohol and their derivatives as reaction medium.

K. S. Park · C. H. Song · A. M. Stephan · S. K. Jeong · K. S. Nahm (✉)
School of Chemical Engineering & Technology,
Chonbuk National University,
Jeonju, Seoul 561-756, South Korea
e-mail: nahmks@chonbuk.ac.kr

S. M. Oh · Y. G. Kim
Department of Chemical Technology,
College of Engineering, Seoul National University,
Seoul 151-742, South Korea

To the best of our knowledge, however, not much attention has been paid on the synthesis of solid solutions with layered manganese oxides by using alcohols and their derivatives as a reaction medium in the solid-state method, as we employ in this work.

In the present study, we synthesized $Li[Li_{1/5}Ni_{1/10}Co_{1/5}Mn_{1/2}]O_2$ solid solution using ethanol or acetone as a reaction medium in the solid-state reaction. In order to understand the reaction chemistry between starting materials and solvent medium in the solid-state reaction, the solid solution was prepared as functions of functional group of starting materials (hydroxide or acetate) and solvent medium (ethanol or acetone). An attempt has also been made to study the structural and electrochemical properties of the synthesized solid solutions.

Experimental procedure

Preparation of $Li[Li_{1/5}Ni_{1/10}Co_{1/5}Mn_{1/2}]O_2$ with starting materials having OH functional group

Stoichiometric amounts of lithium hydroxide (LiOH), nickel hydroxide ($Ni(OH)_2$), cobalt hydroxide ($Co(OH))_2$), and manganese hydroxides (MnOOH) were mixed with a cation ratio of Li:Ni:Co:Mn = 6/5:1/10:1/5:1/2 for the preparation of $Li[Li_{1/5}Ni_{1/10}Co_{1/5}Mn_{1/2}]O_2$. In order to enhance the solid-phase diffusion, the mixture was ground for 4 h using the zirconia ball miller with and without the addition of solvent (0.5 cc/g of solid). Since the ball milling was allowed only for 4 h we did not observe any kind of impurity in the structure of the end product. Sample A was prepared without solvent, whereas samples B and C were synthesized with the addition of ethanol and acetone, respectively. The ground powder mixture was pre-calcined at 600°C for 10 h, followed by the post-calcination at 940°C in air for 10 h after grinding the pre-calcined samples.

Preparation of $Li[Li_{1/5}Ni_{1/10}Co_{1/5}Mn_{1/2}]O_2$ with starting materials having COO functional group

The $Li[Li_{1/5}Ni_{1/10}Co_{1/5}Mn_{1/2}]O_2$ was prepared with starting materials having acetate functional group, lithium acetate ($CH_3COOLi \cdot 2H_2O$), nickel acetate ($(CH_3COO)_2Ni \cdot 4H_2O$), manganese acetate ($(CH_3COO)_2Mn \cdot 4H_2O$), and cobalt acetate ($(CH_3COO)_2 \cdot Co$) with a cation ratio of Li:Ni:Co:Mn = 6/5:1/10:1/5:1/2. The rest of the processes were the same as described in the previous section. Sample D was prepared without the solvent addition, whereas samples E and F were synthesized with the addition of ethanol and acetone, respectively.

Characterization of prepared $Li[Li_{1/5}Ni_{1/10}Co_{1/5}Mn_{1/2}]O_2$ materials

The structure of the prepared powders was characterized using a X-ray diffraction (D/Max-3A, Rigaku XRD) with a CuKα radiation. Raman spectra were taken between 100 cm^{-1} and 900 cm^{-1} at room temperature in a quasi-back scattering configuration. A Renishaw micro-Raman Spectrometer (RENISHAW Co.) with holographic gratings and a computer controlled photon-counting system was used for this purpose. The laser light source was 514 nm line radiation from a Spectra-Physics 2020 argon-ion laser. To attain a high signal-noise ratio, each Raman spectrum was taken by averaging 6 successive scans obtained at a spectral resolution of 2 cm^{-1}. The frequency stability and the accuracy of the apparatus were checked by recording the Raman spectrum of silicon. To avoid sample photodecomposition or denaturation, Raman spectra were recorded using a low excitation power of 20 mW. An increase in lattice temperature generally results in a shift of Raman peak wave-number up to the formation of Mn_3O_4 oxide. All powders were palletized to obtain a mirror-like surface sample for the Raman analysis. The electrochemical characterization was carried out using CR2032 coin-type cells. The detailed description for the cell fabrication was reported elsewhere [11, 12]. The charge and discharge processes were carried out at a current density of 0.8 mA/cm^2 (40 mAh/g) with a cut-off voltage range of 2.5–4.5 V (versus Li/Li^+).

Results and discussion

Figures 1(a), (b), (c), (d), (e), and (f) show the XRD patterns for samples A, B, C, D, E, and F, respectively. All the peaks appearing in the XRD patterns of the prepared samples were identified with the characteristic peaks reported in the X-ray powder data file of JCPDS [13], based on a hexagonal α-$NaFeO_2$ structure (space group: R $\bar{3}$m, 166). The superlattice ordering peaks were observed between 20° and 25° (in the rectangle), resulting from the short-range ordering of Li, Ni, Co, and Mn atoms on the transition metal layers [12, 14]. The clear splitting of the lines assigned to Miller indices (006), (102), and (108), (110) is a

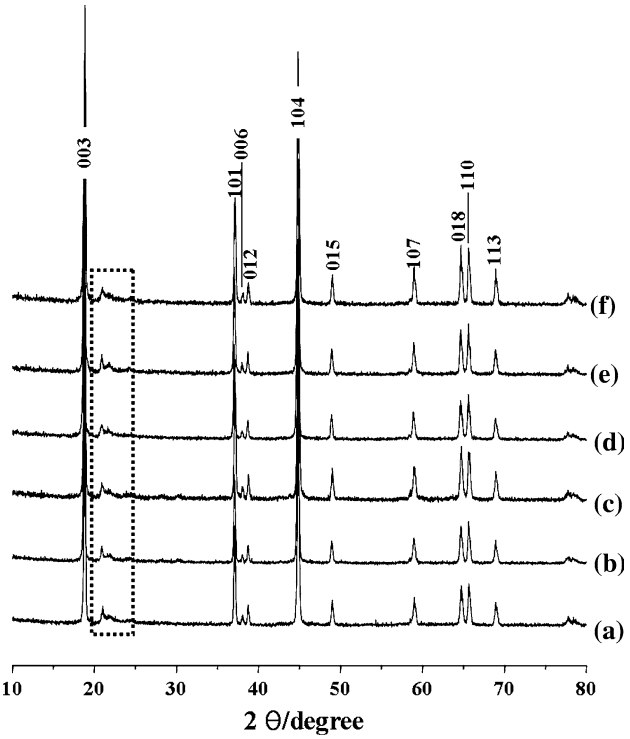

Fig. 1 X-ray patterns for $Li[Li_{1/5}Ni_{1/10}Co_{1/5}Mn_{1/2}]O_2$ (**a**) prepared by hydroxide without solvent (pellet), (**b**) prepared by hydroxide with alcohol (powder), (**c**) prepared by hydroxide with acetone (powder), (**d**) prepared by acetate without solvent (pellet), (**e**) prepared by acetate with alcohol (powder), and (**f**) prepared by acetate with acetone (powder)

characteristic peak of typical layered structure. Morales et al. [15] and Ohzuku et al. [16] reported that the (003) peak occurs from the diffraction of the layered rock-salt structure (R $\bar{3}$m), whereas the (104) peak appears from both the diffractions of layered and cubic rock-salt structures. It is generally reported that layered cathode materials produce good electrochemical properties when the intensity ratio of (003) and (104) peaks is higher than 1.2, and further more the (101), (006), and (108) (110) peaks are clearly split. According to Hwang et al. [17] the intensity ratio of the (003) and (104) peaks can be used as tool to identify the cation mixing and undesirable cation mixing takes place when the value of intensity ratio is less than 1.2. In the present study, the $I(003)/I(104)$ ratio of the samples is higher than 1.2, which further substantiates that all synthesized materials are layered in structure. Table 1 depicts the values of c/a for all the samples which vary from 4.996 to 4.999, which indicate that the prepared materials are not cubic [18] and the values are the same irrespective of the materials used during the synthesis process.

Figure 2 shows the capacity versus voltage profile of the cell comprising Li/$LiPF_6$-EC/DMC(1:2 by vol.)/ $Li[Li_{1/5}Ni_{1/10}Co_{1/5}Mn_{1/2}]O_2$ at room temperature. The measured data show monotonic discharge curves with one step, which is a characteristic feature of typical layered structure. It is interesting to note, that the solvents used during the synthesis process play an important role having hydroxide functional group, while on the other hand, any discernable changes could not be seen on the discharge capacity of the samples prepared with acetate functional group. Among the samples prepared with hydroxide functional group (samples A, B, and C), the addition of solvents with the starting material considerably increases the discharge capacity of the system. The sample B which was prepared with ethanol delivers higher discharge capacity than the sample C prepared with acetone as solvent (Fig. 2(b), (c)). On contrary, the solvent effect is negligible for the samples prepared with the starting materials having acetate functional group (Fig. 2(d–f)). It is seen from the figure that the samples A, B, C, D, E, and F offer the irreversible capacity of 48, 129, 87, 129, 122, and 125 mAh/g, respectively, and is attributed to either oxygen loss or extraction of Li ion on the transition metal layers. Interestingly, the length of the irreversible capacity for sample A is shorter than other samples studied. It was reported that the irreversible capacity affects on the electrochemical performance, such as discharge capacity and cycling performance. The materials with higher irreversible capacity exhibit an increase of the initial capacities, resulting in the

Table 1 Lattice parameters, *R*-factor and discharge capacities of synthesized at different conditions

Sample	Starting materials	Solvents	Lattice parameter			*R*-factors		Discharge capacities (mAh/g)			
		No	*a*	*c*	*c*/*a*	R_p	R_w	1st cycle	Maximum (cycle)	45th cycle	Capacity fading (%/cycle)
A	Hydroxide	No	2.846	14.219	4.996	14.8	18.6	107	141 (18)	137	0.063
B		Ethanol	2.846	14.219	4.996	14.5	17.8	140	184 (13)	173	0.016
C		Acetone	2.846	14.220	4.996	15.3	14.0	119	154 (11)	153	0.014
D	Acetate	No	2.845	14.221	4.999	12.2	13.2	173	207 (12)	199	0.086
E		Ethanol	2.846	14.223	4.998	10.8	11.8	155	196 (12)	190	0.057
F		Acetone	2.846	14.224	4.998	14.2	11.7	158	204 (17)	199	0.055

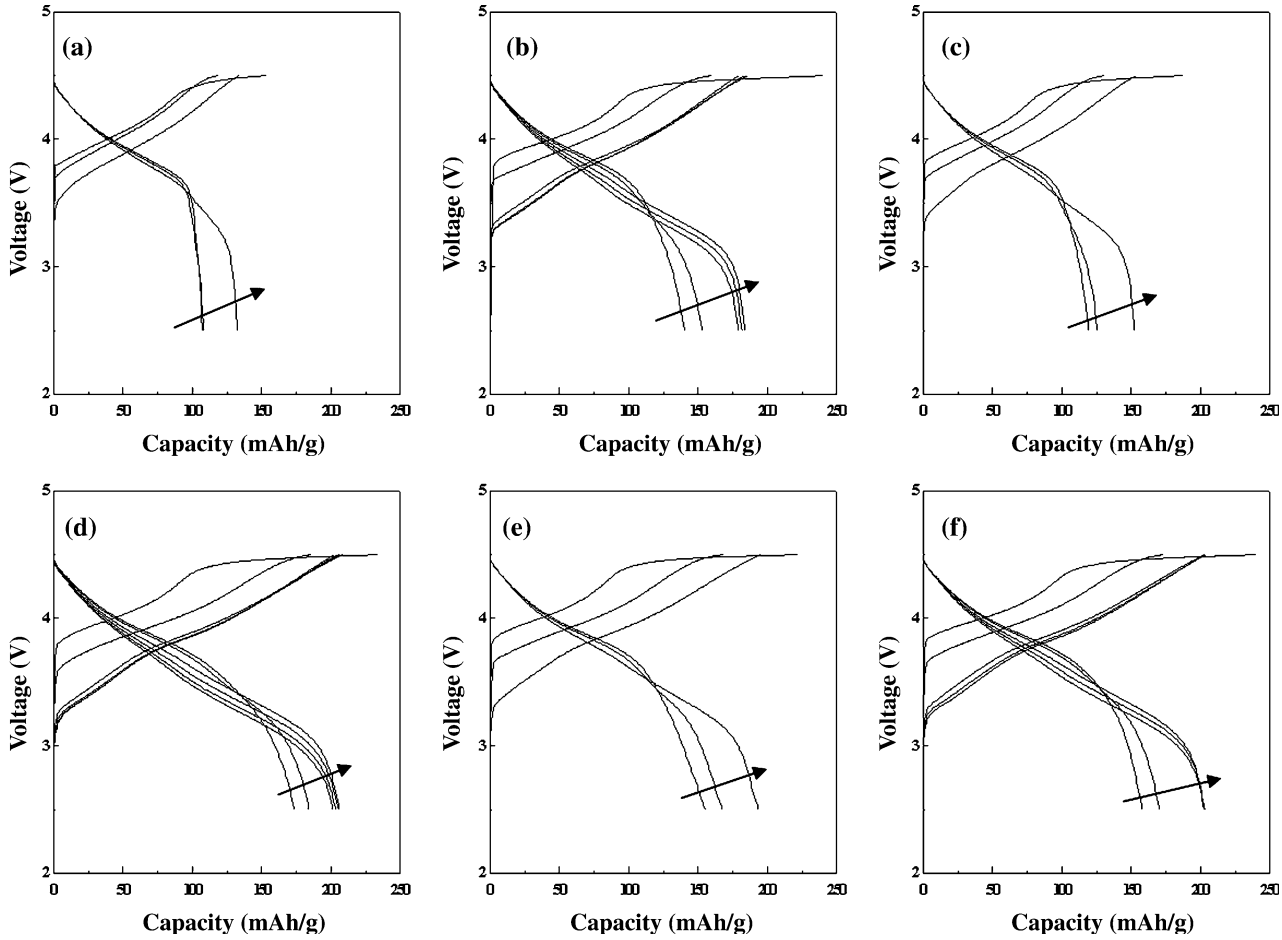

Fig. 2 Plots of voltage versus capacity for $Li[Li_{1/5}Ni_{1/10}Co_{1/5}Mn_{1/2}]O_2$ (**a**) prepared by hydroxide without solvent (pellet), (**b**) prepared by hydroxide with alcohol (powder), (**c**) prepared by hydroxide with acetone (powder), (**d**) prepared by acetate without solvent (pellet), (**e**) prepared by acetate with alcohol (powder), and (**f**) prepared by acetate with acetone (powder) measured in the voltage range of 2.5–4.5 V

delivery of higher discharge capacity. A similar trend was observed for all the samples studied.

Figure 3 shows the discharge capacities as a function of cycle number for the cells comprising Li/$LiPF_6$-EC/DMC (1:2 by vol.)/$Li[Li_{1/5}Ni_{1/10}Co_{1/5}Mn_{1/2}]O_2$ at room temperature. The initial discharge capacities of samples A, B, C, D, E, and F are 107, 140, 119, 173, 155, and 158 mAh/g, respectively. The discharge capacity gradually increases with the increase of cycle number at the initial stage. The discharge capacities of the samples A, B, C, D, E, and F are 137, 173, 153, 199, 190, and 199 mAh/g and their corresponding fade in capacity is 0.063, 0.016, 0.014, 0.086, 0.057, and 0.055 mAh/g, respectively, after 45 cycles. The initial increase of discharge capacities with cycle number has generally been observed in the layered manganese oxide solid solutions with Li ion in their transition metal layers [1, 3, 4, 12, 14] and is attributed to the stabilization of synthesized solid solutions with cycling [1] or due to the change of Mn oxidation state from 4+ to 3+ (during discharge process) or from 3+ to 4+ (during charge process) during cycling [3], or due to the contribution of lithium ions removed from transition metal layers while cycling [4, 12, 14]. However, the increase of capacity upon cycling has not yet been clearly understood. Hence, it appears that as a general consensus these materials have extremely complex structures.

Generally, it is suggested that the irreversible capacity during the 1st charge is concerned with theoretical capacity and the structural stability. It is quite obvious from Fig. 2 except for the sample A, the voltage plateau of the charging capacity is about 100 mAh/g for all the samples studied. It means that the charging capacity of sample A due to the presence of the redox couple Ni^{2+} to Ni^{4+}, and for the other samples (B–F) it is either due to the oxygen loss or extraction of Li ion on the transition metal layers. The

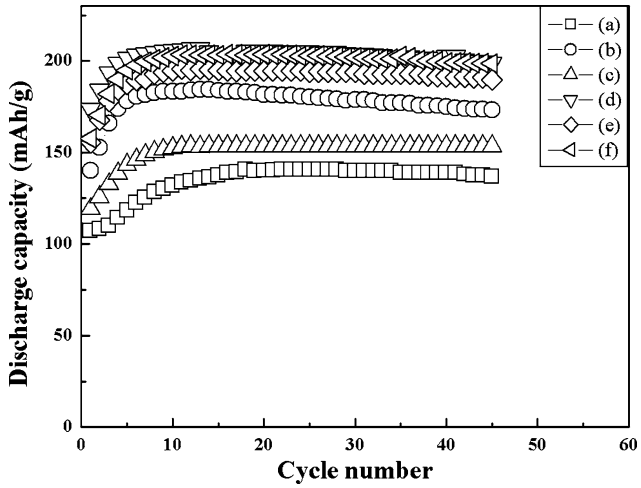

Fig. 3 Plots of capacity versus cycle number for $Li[Li_{1/5}Ni_{1/10}Co_{1/5}Mn_{1/2}]O_2$ (**a**) prepared by hydroxide without solvent (pellet), (**b**) prepared by hydroxide with alcohol (powder), (**c**) prepared by hydroxide with acetone (powder), (**d**) prepared by acetate without solvent (pellet), (**e**) prepared by acetate with alcohol (powder), and (**f**) prepared by acetate with acetone (powder)

extraction of Li ion from the transition metal layers [4] makes electron unstable at higher voltage region (over 4.45 V). This results a change in the oxidation state of manganese to keep the electroneutrality and oxidation change of Mn during cycling also increases the discharge capacity.

Several researchers employed different routes for the synthesis of $LiMnO_2$ and its derivatives. For example, Shaju et al. [19] prepared $LiNi_{1/3}CO_{1/3}Mn_{1/3}O_2$ using the mixed hydroxide method. Although, the authors found an initial capacity of 140 mAh/g, upon 30 cycles the materials show a fade in capacity of 1.3 mAh/g per cycle. Further more, precursors need to be calcined at 1000 °C. In a similar way, Lu and Dahn [20] synthesized $Li[NiLi_{1/3-2x/3}Mn_{2/3-x/3}]O_2$ by mixed hydroxide method that also showed an initial capacity of 140 mAh/g. Cho et al. [21] reported the synthesis of $Li(Ni_{1/3}Mn_{1/3}Co_{1/3})O_2$ as an insertion cathode material by carbonate co-precipitation method. The $Li[(Ni_x Li_{(1/3-2x/3)}Mn_{(2/3-x/3)}]$ compound was prepared by Park et al. [22] by simple combustion method. Although these samples exhibited an initial capacity as high as 200 mAh/g the fade in capacity per cycle is found to be 1.6 mAh/g.

It is worthy to note that many researchers applied hydroxide co-precipitation method [4, 23, 24]. In this method, the Mn ion is precipitated $Mn(OH)_2$ (Mn is 2^+) but oxidized gradually, so valence state changed to $Mn3^+$ (MnOOH) or $Mn4^+$ (MnO_2) in aqueous solution. Therefore reproducibility of the precursor is very difficult. So the procedure adopted herein shows (sample f) the discharge capacity as high as 200 mAh/g and its fade in capacity was found to be 0.055 mAh/g after 45 cycles.

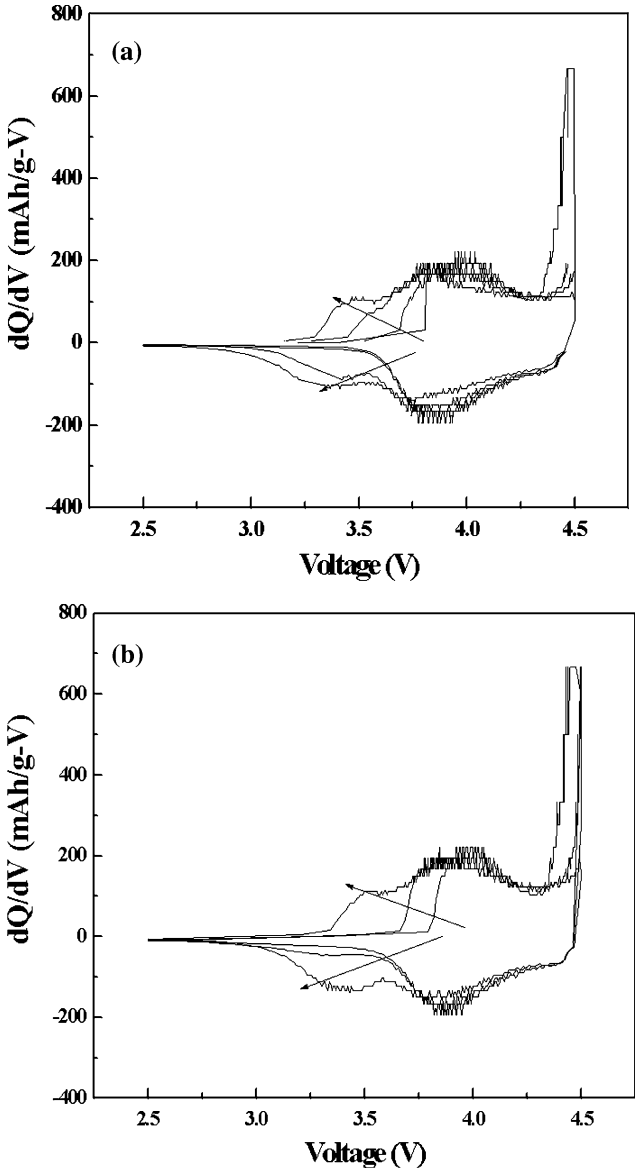

Fig. 4 Differential capacity versus potential for $Li[Li_{1/5}Ni_{1/10}Co_{1/5}Mn_{1/2}]O_2$ (**a**) sample A and (**b**) sample C

In order to clearly understand oxidation change of Mn, we measured the dQ/dV for varying the applied voltage. Typically, the dQ/dV versus voltage curve between 2.5 V and 4.5 V for samples A and C are shown in Fig. 4(a) and (b), respectively. In the charging process, the broad peak observed between 3.7 V and 4.1 V are due to the oxidation of Ni^{+2} to Ni^{+4} in the material. A dramatic increase in oxidation peak appears above 4.46 V and is due to the irreversible capacity plateau observed at the 1st cycle in Fig. 2. At

the 1st charge process, however, the oxidation peak from Mn^{+3} to Mn^{+4}, which arises below 3.5 V, is not observed in all samples. This indicates in the as-prepared samples the oxidation state of Mn is +4. But the Mn oxidation peak begins to appear after the 3rd charge process. The peak observed at 3.26 V is due to the oxidation of Mn^{3+} produced by the partial reduction of Mn^{4+} at the 1st discharge process. The oxidation of Ni^{2+} to Ni^{4+} occurs at 3.74 V, which is shifted from the voltage value shown at the first charge. After the third cycle, the charge and discharge curves are almost same in the shape for the all other cycles. But the peak positions slightly shift at the initial steps, resulting in the increase of the capacity, and are saturated upon cycling. The above observation clearly demonstrates that not only Ni but also Mn in the synthesized sample, $Li[Li_{1/5}Ni_{1/10}Co_{1/5}Mn_{1/2}]O_2$ are responsible for the oxidation and reduction processes during the cycling.

Figure 5(a–f) shows the Raman scattering spectra of samples A, B, C, D, E, and F, respectively. For all samples except samples A and C, the three Raman-active modes of $Li[Li_{1/5}Ni_{1/10}Co_{1/5}Mn_{1/2}]O_2$ are assigned at 430, 482, and 595 cm^{-1}, although the intensities of the samples are a little bit different. The Raman spectra are well agreed with the factor group analysis of the R $\bar{3}$m symmetry except peak at 430 cm^{-1}. The peaks at 482 cm^{-1} and 595 cm^{-1} are attributed to the Raman-active species E_g and A_{1g}, respectively. The appearance of the Raman bands are likely due to the motions involved in the M–O stretching and O–M–O bending, as the contributions of the Raman modes are only from the vibrations of oxygen atoms. The A_{1g} mode has the greater oscillator strength and that the intensity is twice that of the E_g mode [25].

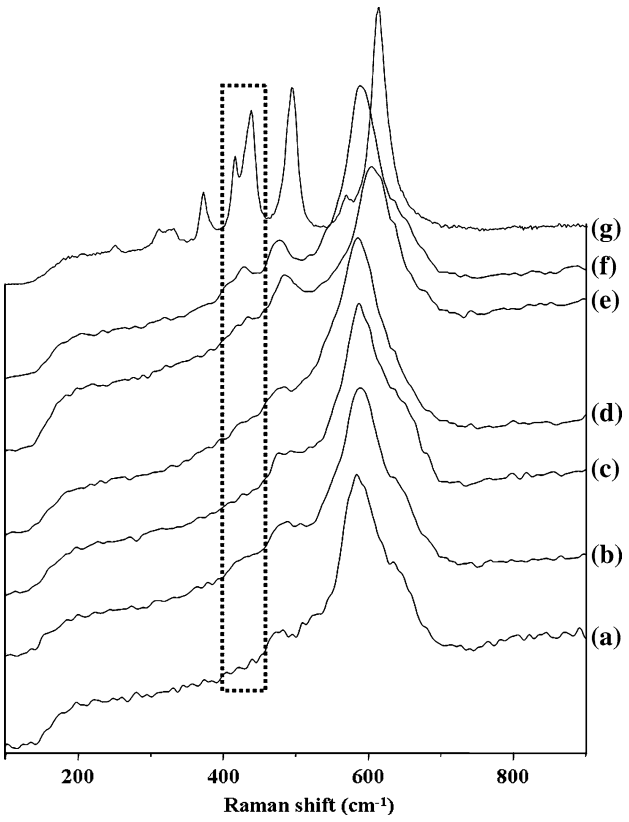

Fig. 5 Raman spectra for $Li[Li_{1/5}Ni_{1/10}Co_{1/5}Mn_{1/2}]O_2$ (**a**) prepared by hydroxide without solvent (pellet), (**b**) prepared by hydroxide with alcohol as solvent (powder), (**c**) prepared by hydroxide with acetone as solvent(powder), (**d**) prepared by acetate without solvent (pellet), (**e**) prepared by acetate with alcohol as solvent (powder), (**f**) prepared by acetate with acetone as solvent(powder), and (**g**) Raman spectrum for Li_2MnO_3

The Raman peak that appears at 430 cm^{-1} is attributed to the presence of Li_2MnO_3 superlattice. The XRD peaks between $2\theta = 20°$ and 25° also correspond to this [12, 14]. Figure 5(g) represents the Raman spectrum of Li_2MnO_3 for comparison. The structure of Li_2MnO_3 is a rock-salt configuration in which layers of lithium ions and layers of manganese and lithium ions (in a 1:2 ratio) alternatively arranged between the closely packed oxygen planes. The close-packed oxygen array is slightly distorted from the ideal cubic-close-packing. The Li_2MnO_3 structure is similar to the layered structures of $LiCoO_2$ and $LiNiO_2$; it can be represented (in layered notation) as $[Li]_{3a}(Li_{1/3}Mn_{2/3})_{3b}O_2$ in which 3a and 3b refer to the octahedral sites of the trigonal lattice (Wyckoff notation). According to the theoretical calculation, the monoclinic Li_2MnO_3 oxide with C_2H_3 spectroscopic symmetry is predicted to show six Raman-active modes with $4A_g + 2B_g$ species [26, 27]. However, the Raman spectrum of the monoclinic Li_2MnO_3 phase contains experimentally nine main peaks at 248, 308, 332, 369, 413, 438, 493, 568, and 612 cm^{-1}. In the present work due to the over lapping of superlattice or lower intensities due to the short-range ordering of Li, Ni, Co, and Mn atoms on the transition metal layers the only peak at 430 cm^{-1} is observed [28, 29]. In this work, the samples except samples A and C produce the superlattice peak at 430 cm^{-1} in Raman spectra. This result is reflected on the electrochemical properties of materials also. Samples B, D, E, and F with the superlattice peak show higher irreversible capacity. It is considered that the extraction of Li ion changes the oxidation state of Mn ion on the transition metal layers, resulting in an increase of the irreversible capacity. It means that the superlattice affects the irreversible capacity. It is considered that the magnitude of the irreversible capacity is influenced by the structure of the synthesized materials, although they were synthesized under the same composition and condition. The

trends of irreversible capacities and discharge capacities of the synthesized samples varied in the following way.

$$\text{SampleB} = \text{sampleD} > \text{sampleF} > \text{sampleE} > \text{sampleC} > \text{sampleA}$$

Sample A delivered very low irreversible capacity and discharge capacity. It seems that the oxidation state of Mn ion in the sample is hardly changed during cycling.

Samples B, D, E, and F show peaks of A_{1g} mode at 595 cm^{-1}, E_g mode at 482 cm^{-1}, and superlattice peak at 439 cm^{-1}, respectively. The supperlattice peaks are not observed from the Raman spectra of samples A and C. It means that the stoichometries of the samples B, D, E, and F are very close to the standard values in the Raman analysis, compared to samples A and C.

Obviously, these results indicate that the materials with hydroxide functional groups are more dependent on solvents, whereas the effect of solvent is not predominant for the materials with acetate functional group.

The discharge capacities of the materials prepared with hydroxide functional group added with solvents are greatly varied with the samples without solvent. In the solid-state reactions, the diffusion rate of chemical species might be poor during the synthesis process, because the solid-phase diffusion of the chemical species during the solid solution state synthesis occurs mainly by the mechanical mixing or by ball milling and the calcination temperature. Poor diffusivities of the components in the solid-state reactions might cause the formation of unstable structured materials, resulting in poor electrochemical properties [30, 31].

While synthesizing the samples with the addition of solvents enhances the diffusivity of the chemical species or influence the chemical reaction during the synthesis [32]. In the presence of ethyl alcohol, lithium hydroxide reacts with the alcohol and forms lithium alkoxide (LiOR), as depicted in Eq. 1.

$$\mathrm{Li^+OH^-} \cdot x\mathrm{H_2O} + \mathrm{RO\text{-}H} \leftrightarrow \mathrm{RO^-Li^+} + x\mathrm{H_2O} \quad (\mathrm{R}: \mathrm{CH_3CH_2^-}) \tag{1}$$

LiOH dissociates into Li^+ and OH^- and, similarly, ethyl alcohol decomposes into RO^- ($CH_3CH_2O^-$) and H^+. During the reaction, negatively charged RO^- will combine with the positively charged Li^+ ion and forms LiOR. On the other hand the OH^- ion will combine with H^+ ion forms water molecules. However, this reaction is reversible. The forward reaction is more favorable than the reverse reaction, because LiOH is a stronger base than LiOR. The LiOR participates in the reaction of $Ni(OH)_2$, $Co(OH)_2$, and MnOOH to form $Li[Li_{1/5}Ni_{1/10}Co_{1/5}Mn_{1/2}]O_2$.

$$5/6\mathrm{LiOR} + 1/10\mathrm{Ni(OH)_2} + 1/5\mathrm{Co(OH))_2} + 1/2\mathrm{MnOOH} \rightarrow \mathrm{Li[Li_{1/5}Ni_{1/10}Co_{1/5}Mn_{1/2}]O_2} + 5/6\mathrm{RO\text{-}H} + x\mathrm{H_2O} \tag{2}$$

In the case of acetone added materials, the acetone looses its hydrogen under strong base condition to be negatively charged. Since the negatively charged species is more reactive than acetone, it may attack neighbor acetone to form alkoxide. This can easily combine either with proton released from acetone or Li ion ionized from LiOH to form the corresponding alcohol or lithium salt in equal ratio (see Eq. 3). Because of these reactions the ratio of lithium salt to the amount of material synthesized is lesser than 50%.

Consequently, the probability of formation of lithium salt is lower in acetone than in alcohol. It means the chances for the formation of a sample with stable structure is higher in alcohol than in acetone. From these results, the samples prepared with ethyl alcohol delivered higher discharge capacity than the samples prepared with acetone when the starting materials have hydroxide functional group.

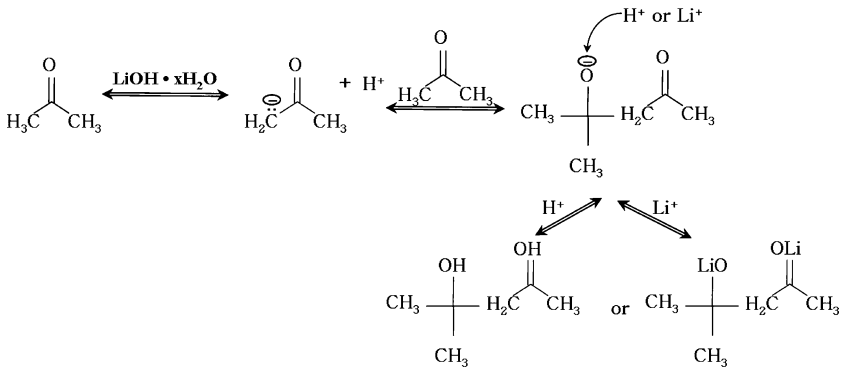

But, when the starting materials have acetate functional group, the chemistry of solvent and starting materials are different from that of starting materials with hydroxide functional group. Hydroxides are dissolved in water, whereas acetates not dissolved in water. But the acetates unreact with ethyl alcohol and acetone, meaning that ethyl alcohol and acetone do not participate in the chemical reaction. It seems that water is extracted from starting materials due to vigorous mixing using a ball miller. Then the starting materials with acetate functional group may be dissociated into carboneous groups and their metal ions in water. This allows a homogeneous mixing of the starting materials, resulting in a high reactivity of the mixture. Therefore, the samples prepared from the starting materials with acetate functional group show almost similar structural and electrochemical properties, irrespective of the solvent used.

Conclusion

The layered compound, $Li[Li_{1/5}Ni_{1/10}Co_{1/5}Mn_{1/2}]O_2$ was synthesized by solid-state reaction method with starting materials having two different functional groups (hydroxide or acetate) in the presence of a reaction medium (ethanol or acetone). The prepared samples were of layered in structure and the samples prepared with ethanol offered higher discharge capacity than those prepared with acetone. All samples showed a gradual increase in the discharge capacity with cycle number. The addition of solvents during the synthesis process considerably enhances the diffusivity of the chemical species and also offered materials with better electrochemical properties.

Acknowledgements This work was supported by the Energy Conversion and Storage Research Center through the Ministry of Science and Technology.

References

1. Kim JH, Sun YK (2003) J Power Sources 119–121:166
2. Lu Z, Dahn JR (2002) J Electrochem Soc 149:A1454
3. Kang SH, Sun YK, Amine K (2003) Electrochem Solid State Lett 6:A183
4. Kang SH, Amine K (2003) J Power Sources 124:533
5. Lu Z, Macneil KK, Danh JR (2001) Electrochem Solid State Lett 4:A200
6. Jouanneau S, Macneil DD, Lu Z, Beattie SD, Murphy G, Dahn JR (2003) J Electrochem Soc 150:A1299
7. Lu Z, Beaulieu LY, Donaberger RA, Thomas CL, Dahn JR (2002) J Electrochem Soc 149:A778
8. Johnson CS, Kim JS, Kropf AJ, Kahainan AJ, Vaughey JT, Fransson LLM, Edstrom K, Thackerfay MM (2003) Chem Mater 15:2313
9. Lee YS, Satoy S, Sun K, Kobayakawa K, Sato Y (2003) Electrochem Commun 5:359
10. Sakurai Y, Arai H, Yamakaki M (1998) Solid State Ionics 113–115:29
11. Sakurai Y, Arai H, Okada S, Yamaki JI (1997) J Power Source 68:711
12. Park KS, Cho MH, Jin SJ, Nahm KS, Hong YS (2004) Solid State Ionics 171:141
13. Park SH, Park KS, Sun YK, Nahm KS, Lee YS, Yoshio M (2001) Electrochim Acta 46:1215
14. Park KS, Cho MH, Jin SJ, Nahm KS (2004) Electrochem Solid State Lett 7:A239
15. Morales J, Peres-Vicnete C, Tiranto JL (1990) Mater Res Bull 25:623
16. Ohzuku T, Ueda A, Nagayama M (1993) J Electrochem Soc 140:1862
17. Hwang BJ, Santhanam R, Chen CH (2003) J Power Sources 114:244
18. Bruce PG, Armstrong AR, Gitzendanner RL (1999) J Mater Chem 1:193
19. Shaju KM, Subba Rao GV, Chowdari BVR (2002) Electrochim Acta 48:145
20. Lu Z, Dahn JR (2002) J Electrochem Soc 149:A815
21. Cho TH, Park SM, Yoshio M, Hirai T, Hideshima Y (2005) J Power Sources 142:306
22. Park JY, Hong YS, Wu X, Ryu KS, Chang SH (2004) J Power Sources 129:288
23. Yabuuchi N, Ohzuku T (2003) J Power Sources 119–121:171
24. Macneil DD, Lu Z, Dahn JR (2002) Electrochem Soc 149:A1332
25. Julien C, Camacho-Lopez MA, Mohan T, Chitra S, Kalyani P (2000) Solid State Ionics 135:241
26. Julien CM, Massot M (2003) Mater Sci Eng B100:69
27. Chang CC, Kumta PN (1998) J Power Sources 75:44
28. Castro-Garcia S, Castro-Coucerio A, Senari-Roddriguez A, Soulette F, Julien C (2003) Solid State Ionics 156:15
29. Rao RCN (1999) J Mater Chem 9:1
30. Lu Z, Maccneil KK, Dahn JR (2001) J Electrochem Solid State Lett 4:A191
31. Park SH, Sun YK (2003) J Power Sources 119–121:161
32. Lu Z, Beailieu LY, Donaberger RA, Thomas CL, Dahn JR (2002) J Electrochem Soc 149:A778